Semi-empirical model for predicting LAB and HAB formation in Bearing Steels

Mostafa El Laithy[a], Ling Wang[a], Terry J. Harvey[a], Bernd Vierneusel[b]

[a]*National Center of Advanced Tribology at Southampton (nCATS), University of Southampton, University Road, Southampton SO17 1BJ, UK*

[b]*Schaeffler Technologies AG & Co. KG, Georg-Schäfer-Straße 30, 97421 Schweinfurt, Germany*

Abstract

The formation of white etching bands (WEBs), including both low- (LAB) and high- (HAB) angle bands, in the subsurface of steel bearings due to rolling contact fatigue (RCF) has been investigated over decades to understand their characteristics and predict their formation during operation. A few studies recently have modelled the development of LABs theoretically based on thickening of lenticular carbides adjacent to the band controlled by dislocation-assisted carbon migration. To date, no study has been reported to predict the formation of HABs. Based on the percentage of white etched region formed in the subsurface of the bearings, this study presents a semi-empirical model that predicts the formation of both LABs and HABs in steel bearings for different contact pressures. The LAB semi-empirical model is compared with a theoretical model from literature and experimental data. According to this, the new model more realistically predicts the initiation of LABs than the carbide thickening model. This is achieved by involving the formation of ferrite (cellular and elongated) shown as white areas under optical images. Literature data have been used to evaluate the LAB and HAB models. The growth pattern obtained in this study provides strong evidence of a diffusion-based mechanism leading to WEB formation.

1. Introduction

Microstructural alterations, such as dark etching regions (DER) and white etching bands (WEBs), found in the subsurface of steel bearings as critical material degradation stages under rolling contact fatigue (RCF) have been investigated for decades. However, the conditions controlling their development and their formation mechanisms are still being been debated [1, 2] . Furthermore, there is a lack of precise predictive models for these features.

DER is observed in optical images as dark patches in bearing subsurface when etched with Nital (2% nitric acid + 98% ethanol) within the region of the maximum shear stress, formed beyond 5 million stress cycles [2]. WEBs,

including low angle bands (LABs) and high angle bands (HABs), are developed later in the bearing life compared to DER. They also develop in the region of the maximum shear stress [3], and hence typically found within the DER however some have reported to have developed without DER if the material is tempered to a hardness below 720 HV [4, 5]. LABs form from beyond 100 million stress cycles followed by HABs forming beyond 500 million cycles. LABs are inclined to the surface in the rolling direction at an angle of 20-35° with an average length and thickness of 52 µm and 1.6 µm respectively, while HABs are inclined at 65-80° with an average length and thickness of 60 µm and 5.6 µm respectively [3]. Detailed analysis on the WEBs formed at different stages have shown that the density of WEBs increases with stress cycle [3]. The development of DER and WEBs associated with elemental redistribution of carbon and softening of the microstructure [6, 7, 2] may affect the integrity of the microstructure of bearing steels leading to weak boundary planes in the parent microstructure and contribute to crack propagation [8, 9] and failures. While a better understanding of the formation mechanisms of these features is being investigated, modelling their behaviour to achieve the prediction of WEBs formation is in great need.

DER and WEBs have been associated with a form of tempering of the martensitic microstructure due to RCF [10, 2, 7, 11, 9] and are suggested to be due to the carbon migration from the parent martensite to heavily dislocated regions and nano-sized tempered carbides [7, 2, 12, 13, 14, 10, 9] leading to ferrite formation. Accumulating plastic deformation is believed to have a major role in the formation of these features given a large number of stress cycles is required to form DER, LABs and HABs. The role of plastic deformation is also supported by the observation that no microstructural alterations occur below the contact pressure threshold of 2.5 GPa, i.e. the shakedown limit of the steel [10, 2]. While DER is found to contain dark patches of ferrite grains randomly distributed in the region of the maximum shear stress, WEBs are directional ferrite bands inclined at certain angles to the contact surface. Significant evidence in literature has shown that lenticular carbides (LCs) exist adjacent to the ferrite band of LABs [6, 15].

One of the earliest models presented by Buchwald et al. [14] suggested that carbon flows from the ferrite band of LABs to the parent microstructure due to stress gradient and carbon concentration as the basis of their model for the determination of the rate of LCs thickness increase thus the WEB formation stage. The model proposed that WEBs form due to dilational compressive strains caused by localized plastic deformation and the association of carbon with the increased dislocation density. It was suggested that the hydrostatic pressure under Hertzian contact is sufficient to dissolve precipitates in the matrix which later becomes LABs, resulting in a localized carbon concentration gradient. The carbon migration driven by the resulted carbon concentration gradient and stress gradient from the deformed region (white area) to the undeformed surrounding regions leads to the formation of

LCs at the boundary that acts as a sink for the carbon solute. The LC growth rate is modelled by Buchwald et al. [14] to be equal to the sum of the concentration gradient flux and the pressure gradient flux (see Equation 1).

$$\frac{dX_L}{dt}(C_c - C_0) = D\frac{dc}{dx} + \frac{C_0 D}{RT}\frac{dv}{dx} \quad (1)$$

Where the LC growth rate is $\frac{dX_L}{dt}$, C_0 is the carbon concentration at the WEB boundary, C_c is the carbon concentration in the LC, D is the diffusion coefficient of carbon in ferrite, $\frac{dc}{dx}$ is the concentration gradient in the WEB at the moving boundary and $\frac{dv}{dx}$ is the potential gradient caused by pressure gradient at the moving boundary. In this model the carbon concentration gradient is assumed to be linear, i.e. the change between C_c and C_0 over the WEB thickness is linear, while the potential gradient is approximated as the elastic strain energy accompanying the precipitation of a mole of carbide over the WEB thickness. The model by Buchwald et al [14] requires a temperature increase of 200 K maintained between stress cycles in the subsurface, which is yet to be proven to be true in experimental findings. The diffusion rate in this model is too low to explain experimental observations.

Swahn et al. [11] created a simple plot to predict the formation of DER, LAB and HABs based on 80 RCF tests of bearings under the contact pressure between 3.2 and 3.7 GPa in 1970s. By determining the earliest stage of formation for each feature at the two pressures, a linear relation was applied to predict formation of DER, LAB and HAB under other pressures between the two tested pressures. However, it is difficult the determine whether the relationship is actually linear between the two points which causes some uncertainty in the feature prediction. As many subsequent works have shown, the model can only provide roughly guidance on the formation of these features even under the limited contact pressure range. A more precise model is thus required specially for the prediction of the initiation of these features under a wide range of bearing operating conditions and materials.

Polonsky et al. [1] proposed a model linking the WEBs to recrystallisation due to a diffusion mechanism where carbon diffuses from the ferrite band and becomes trapped at dislocations or precipitates as layers of LCs. It was also suggested that primary carbides dissolve within the ferrite bands of LABs due to compressive strain arising from localized plastic deformation. While the model by Polonsky et al. [1] focused on the investigation of WEB orientations, it proposed that the driving force for carbon outflow is likely the stress induced release of carbon segregated at dislocations rather than the carbon solute concentration gradient in the WEB due to dissolving precipitates as proposed by Buchwald et al. [14]. Polosnky et al. [1] suggested that during operation, a quasi-equilibrium environment is achieved, where dislocations become unpinned under high subsurface stress and start multiplying rapidly that is compensated by dislocation annihilation, hence an overall constant dislocation density

is roughly maintained. Dislocation annihilation in this case releases the carbon segregated at dislocations to become free carbon in ordinary solution. However, the relaxation time for the free carbon to re-segregate to the newly created dislocations is much longer than the average time between stress cycles, which is governed by the rotational speed and bearing geometry [1]. Hence concentration of free carbon is increased in the band while the concentration of carbon segregated to dislocations reduces. While all carbon in martensite is assumed to be segregated in the form of dislocation atmospheres given the extremely high dislocation density and hence it is assumed the free carbon in the initial martensitic matrix is low. Therefore, the difference in free carbon concentration between the ferrite band and martensite acts as the driving force for carbon outflow to the edge of the band causing an overall reduction in the carbon content in the band. Based on this hypothesis, Polonsky et al. [1] approximated the number of cycles (N) required to form a carbon free ferrite band of thickness (h) using Equation 2, where D is the diffusion coefficient of carbon in ferrite and n is the rotational speed.

$$N = \frac{h^2 n}{D} \tag{2}$$

This rather simple model has been shown to be insufficient when approximating the number of cycles since it does not take into consideration of the influence of contact pressure, which is known to heavily influence WEB formation. This model was shown to result in values of about a magnitude higher than the experimental data from Buchwald et al. [14]. However, a correction factor of 0.1 to 1 is proposed to account for the fact that, at moderate temperatures, the diffusion coefficient in a heavily dislocated material such as martensite can be considerably higher. Nonetheless, the approximation from this model is closer to the experimental data compared to the initial model by Buchwald et al. [14] which suggests this might be a more realistic formation mechanism.

A more recent study used a finite element (FE) elastic-plastic model coupled with a stress induced carbon diffusion-based model to predict the orientations of the LAB and HABs and to predict the initiation of LABs in the microstructure [16]. The model proposed by Polonsky et al. [1] did not sufficiently deal with the elastic-plastic Hertzian contact. Hence, this recent study developed their model based on the assumption that the dissipated plastic energy during elastic-plastic loading is the primary driver for carbon diffusion, depending on the time span for the diffusion process for each stress cycle, which is also dependent on both bearing speed and geometry. The model has shown to be able to predict LAB formation by predicting the number of cycles required for carbon diffusion across a certain LAB width. The model was based on Fick's first and second law to determine the concentration of a diffusing media under the presence of a pre-existing concentration gradient but the authors modified them to Equation 3 to include stress-assisted diffusion of free carbon.

$$\frac{\partial C}{\partial t} = D\nabla \cdot \left(\nabla c + \frac{c\nabla V}{kT}\right) \quad (3)$$

Where D is the diffusion coefficient of carbon in ferrite, k is the Boltzmann constant, T is temperature, c is the carbon concentration and V is the potential driving the diffusion process which is assumed to be the dissipated plastic energy and ∇ is the Laplace operator.

The FE model showed that the orientation of the diffusional flux to be 25 – 40° in the subsurface depth of about 1 – 1.5b (b is the contact half width) and orientated at 75 – 80° at 0.5 – 1b deep. Indeed the orientations agree with the positioning of LABs and HABs in literature, however this suggests LABs and HABs each have a distinctive region in which they form rather than LABs forming at the depth were HABs would form at a later stage, i.e. HABs consume pre-existing LABs at the same locations. Hence the model could not differentiate the formation of LABs and HABs, which does not agree with experimental observations. Furthermore, since the model was not able to consider stress concentration arising due to carbon diffusion, given that HAB formation is dependent on the stress concentration development due to LAB formation [1] and hence LAB density [3], it could not predict HAB initiation.

Most recently, Fu et al. [7] modelled the formation of DER due to carbon migration through dislocation gliding from the martensite to nano-sized tempered carbides, which leads to carbide thickening and ferrite formation [7]. Based on similar hypothesis, they suggested that, under continuous cyclic loading, the remaining carbon atoms in the newly formed but heavily deformed saturated ferrite will migrate to the edge of the ferrite band due to carbon segregation at dislocations and dislocation gliding, which leads to the nucleation and growth of lenticular carbides (LCs), commonly associated with LABs [13, 6, 14, 2, 17]. The thickening process of LCs was thus modelled as the development state of LABs [13] but no discussions on the formation of HABs were given. The model associates carbon migration with the gliding of dislocations due to plastic deformation in bearing materials under cyclic loading, and the accumulation of stress cycles during bearing operation is treated as a major role in their formation. This is believed a more commendable driving force than that suggested by Buchwald et al., i.e. the migration of carbon is driven by the stress-induced diffusion of free carbon [14].

The dislocation gliding driven carbide thickening process was calculated using the carbon flux equation due to dislocation gliding (Equation 4) and the Orowan equation [18] (Equation 5) for the plastic shear strain rate.

$$J_{dis} = \rho_m \upsilon n_c \quad (4)$$

$$\dot{\gamma} = b\rho_m \upsilon \quad (5)$$

Where J_{dis} is the dislocation assisted carbon flux, ρ_m is mobile dislocation density, υ is an average dislocation velocity, $\dot{\boldsymbol{\gamma}}$ is the plastic shear strain rate, n_c is the number of carbon atoms captured by mobile dislocation of unit length per stress cycle which is estimated using the estimation by Cottrell and Bilby [19] and b is the magnitude of the Burgers vector. Combining Equations 4 and 5, the carbon flux of the system was able to be determined through the measurement of plastic shear strain, avoiding the need of determining the mobile dislocation density and velocity, which is challenging to obtain especially for highly deformed structures such as in bearing steels. While determining the plastic shear strain in bearing steel due to RCF is difficult to obtain, recent studies have approximated such values through compressive cyclic tests. During such tests a decay pattern is observed by comparing the strain at different cycles, suggesting that at high stress cycles (>10^6), the strain range reaches an asymptotic value for each contact pressure [15, 20]. Therefore by developing a linear fitting, the plastic shear strain was approximated for the corresponding contact pressure **[15]**. However there is an uncertainty in this method as the true material response during RCF, given the material softening associated with DER and WEBs may have an impact on the material's plastic shear strain, and thus may deviate from the asymptotic value proposed **[15, 20]**. If there was an increase in its plastic shear strain due to the formation of soft DER and WEB unaccounted for, the proposed model could over-estimate the formation of the WEBs, i.e. predict the formation of WEBs much later than they would actually form. The dislocation assisted carbide thickening model for LABs **[15]** makes use of an equilibrium between the carbon flux towards LC thickening and the dislocation assisted carbon flux shown in Equation 6 and the mass conservation of carbon in the system shown in Equation 7, highlighting the carbon content within the LAB (ferrite region and LC) is equal to the carbon content in the initial matrix over the same area.

$$\boldsymbol{J_{dis} = \frac{dl_{LC}}{dt}\ (C_{v\theta} - C_{v0})} \quad (6)$$

$$\boldsymbol{\lambda C_{v0} = l_{LC} C_{v\theta} + (\lambda - l_{LC})\, C_{vb})} \quad (7)$$

Where $\frac{dl_{LC}}{dt}$ is the rate of thickness increase of the LC, λ is the thickness of a fully developed LAB, $C_{v\theta}, C_{v0}\ and\ C_{vb}$ are the carbon concentration per unit volume in LC, initial matrix and ferrite band respectively and l_{LC} is the thickness of LC. Combining Equations 4 – 7 makes it possible to observe the evolution of carbide thickening due to dislocation assisted carbon diffusion with cycles. According to this model, the estimated maximum thickness of a fully developed LAB was 9 μm [13] . However this has been found to be significantly

larger than that observed by a recent detailed experimental study of LABs [3]. According to Fu et al. [13], carbon flux due to dislocation gliding is many orders of magnitude larger than that due to the concentration gradient of free carbon, it was hence neglected. While this is acceptable, the actual carbon diffusion in the system is most likely to be stress-assisted due to the subsurface stresses acting on the material. Considering a potential gradient across the system that assists the diffusion of free carbon in addition to the carbon flux calculated according to Fick's first law will thus increase the overall flux, similar to that proposed previously [14, 16]. It is thus accepted that both mechanisms, i.e. carbon migration due to dislocation gliding and stress-assisted free carbon diffusion, are likely to contribute to the formation of WEBs and the associated LCs.

However, none of the models could differentiate HABs from LABs that are found to vary in both dimensions and formation at the various stages of bearing life. This is attributed to the fact that no universally accepted theory on the formation mechanism of these features and their transition from DER to LAB and HAB is available. Modelling of carbon migration also requires accurate data such as material plastic shear strain per stress cycle and mobile dislocation density that are extremely difficult to obtain. The estimation of plastic shear strain through monotonic compressive cyclic tests [15, 20], although helpful, its ability to capture the true material response under RCF is questionable. Furthermore, most WEB investigations modelled individual LABs through the adjacent LC thickness, or were not clearly stated, which in practice is near impossible to examine since multiple LABs form simultaneously and appear to be clusters of LABs. Hence the discrepancy in the band thickness adopted in the modelling.

The aim of this study is to develop a working semi-empirical model for the prediction of LABs and HABs formed in steel bearings based on experimental data. A thorough literature review has shown that, the existing LAB models in literature are theoretical models based on LC thickening due to carbon diffusion while no model is available in literature to predict the formation of HABs. Although the theoretical LAB models are all based on carbon migration, conflict modelling results are shown due to the uncertainty in LC thickness measurements used for validation. This is also caused by the simultaneous LABs formation and growth during bearing operation, leading to the large discrepancy in LC thickness quantification and challenges in accurately validating those models. The modelling of WEBs in this study will be based on a larger area of WEBs rather than an individual LAB to eliminate these issues encountered in previous studies. Modelling the LAB formation over a large region globally rather than individual LAB dimensions is proposed to give a more realistic representation of the material behaviour and the WEBs developed. Other microstructural alterations such as white etching areas (WEAs) and white etching cracks (WECs) [3, 21] form in specific regions locally in the microstructure while WEBs occur

more globally on a larger scale, hence it is essential to model the WEB network over the whole microstructure rather than individual bands.

This study takes a novel approach, modelling the WEBs formation and initiation based on quantifying the area consumed by WEBs at different stages (WEBs area is recorded relative to a fixed region and given as a percentage). This technique is conducted to examine how the WEB area grows over a range of bearing operating conditions on several materials. Previous investigations focused on modelling individual band thickness growth on a local scale [14, 15] while the approach in this study models the overall WEB network in the general microstructure on a large scale (hundreds of microns). Most of the experimental data have been presented in a previous publication by the authors [3], this paper will provide some experimental details but will focus on the modelling approach while literature data by other groups are used to validate the semi-empirical models.

2. Experimental Details

A number of RCF tests have been conducted on angular contact ball bearings (ACBBs) 7205B to investigate WEB formation in this study. Three bearing steels were used, including 1) Martensitic 100Cr6 with retained austenite (RA) content of 5%. 2) Bainitic 100Cr6 (RA content 2%) and 3) Martensitic 50CrMo4M (RA content 5%). The chemical compositions of the 100Cr6 (applies to both martensite and bainite microstructures) and 50CrMo4M samples measured, using spark emission spectroscopy, are shown in Table 1. 100Cr6 has been used in this study as the most common bearing steel used in industry. The comparison between the bainitic and martensitic 100Cr6 was conducted to investigate the influence of retained austenite (RA) from 2-5% while the 50CrMo4M was used to investigate the influence of carbon content on the development of LABs and HABs with reference to 100Cr6.

Table 1 Chemical composition of 100Cr6 and 50CrMo4M samples in this study measured using spark emission spectroscopy

	Wt%															
Material	**C**	**Si**	**Mn**	**P**	**S**	**Cr**	**Ni**	**Mo**	**Cu**	**V**	**Al**	**W**	**Pb**	**Sb**	**Ti**	**O**
100Cr6	0.93	0.3	0.34	0.01	0.004	1.49	0.02	0.005	0.066	0.004	0.002	0.007	0.001	0.002	0.001	0.0012
50CrMo4M	0.44	0.24	0.66	0.008	0.001	1.17	0.75	0.25	0.12	0.087	0.024	-	0.001	0.004	0.002	-

All RCF tests were conducted on L-17 test rig (rig details in [21]) at bearing rotating speed of 12000 rpm. The 100Cr6 martensite bearings were tested under both 2.9 and 3.5 GPa while the other two materials were tested under 2.9 GPa only. The oil lubricant (mineral oil) temperature was maintained at 80°C for all tests with a viscosity ratio k of 2.69. Tests were terminated at various pre-determined cycles to allow the investigation of growth of WEBs. Table 2 summarises the test matrix used in this study. After RCF testing, each sample is prepared through

standard metallography **[3]** and analysed through optical microscopy. Optical images from each sample is evaluated using image processing technique to investigate and quantify the relationship between the amount of WEBs and the stress cycles which is used to predict the initiation of LABs and HABs. Details of the test rig, bearing samples and metallography and imaging methods (distinguishing between LABs and HABs in optical images through light polarisation under optical microscope) have been previously detailed in [3]. This paper focuses on the quantification of LABs and HABs and mathematical modelling of their formation processes.

Table 2 A summary of the ACBB tests in this study

Material	Contact Pressure (GPa)	Stress Cycle for Inner Ring ($x10^6$)
100Cr6 Martensite	2.9	591
		1116
		1689
		2341
		3016
	3.5	151
		447
		679
		885
100Cr6 Bainite	2.9	532
		897
		1448
50CrMo4M Martensite	2.9	846
		1626
		2038
		7668

3. Quantification of WEBs

The quantification of WEBs (both LABs and HABs) was conducted by taking optical images of the steel subsurface and processing the images to compare the area of the features to a fixed reference area, e.g. the area view under a light optical microscope (LOM). In this study, an area of 666.7 × 880 μm of the bearing subsurface has been captured by an Olympus BX51 under x20 magnification as shown in Figure 1a.

The area covered by LABs and HABs is measured using ImageJ after the image has been processed as shown in Figure 1b and 1d respectively. The terms LAB% and HAB% are defined as how much of the reference area (666.7

x 880 µm) is covered by LABs and HABs (see Equation 8 for LAB%). For example in Figure 1b, the measured area covered by LABs is 89,764 µm^2 and the total area is 586,696 µm^2 (666.7 × 880 µm). This yields a value for LAB% of 15.

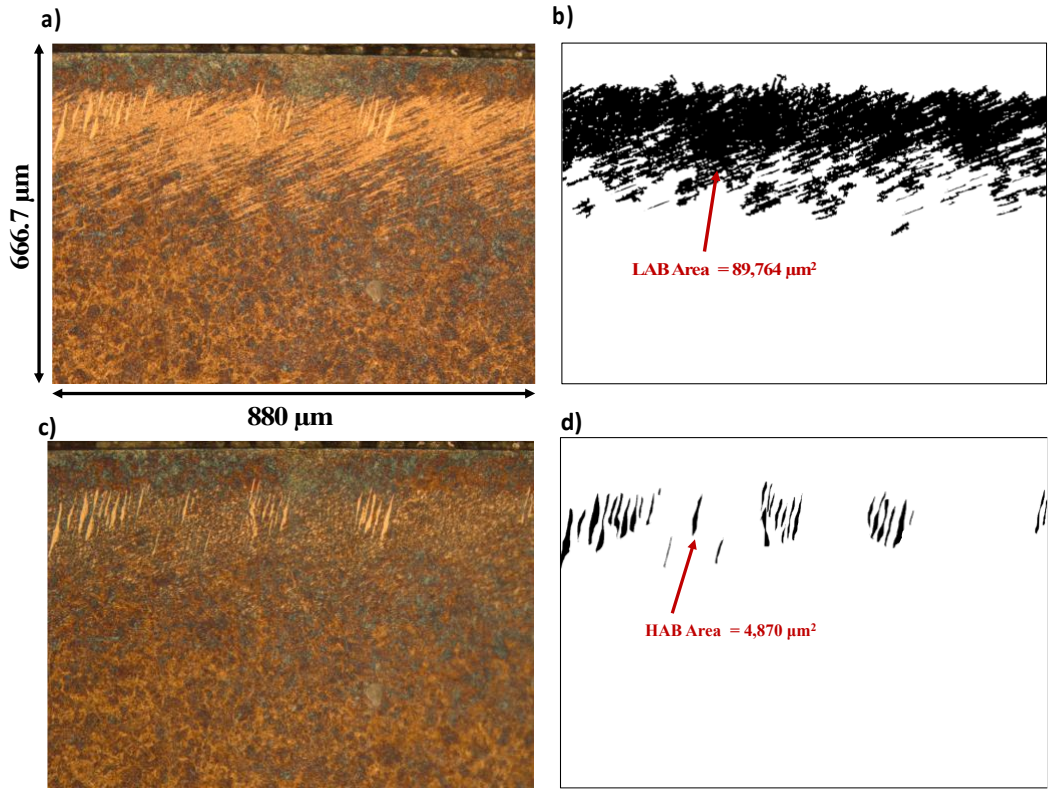

Figure 1a) Optical image of a) LABs and b) HABs showing the area covered by microscope and image processed using ImageJ to measure the b) LAB area and d) HAB area. Features from 100Cr6 martensite sample run at 3016 x10^6 cycles under 2.9 GPa.

$$LAB\% = \frac{LAB\ Area\ \ (black\ area)}{666.7 * 880} \times 100 \qquad (8)$$

The LAB% and HAB% formed in the 100Cr6 (both martensite and bainite) and 50CrMo4M bearings under 2.9 GPa and 3.5 GPa after a range of stress cycles have been quantified using the method detailed in [3] and quickly summarised here is presented in Figure 2. The LAB and HAB formation trends of the 100Cr6 martensite and bainite are shown to be similar under 2.9 GPa, while the 50CrMo4M martensite shows a significant delay in the growth of the LABs and no HABs was found in any of the samples. The influence of increasing the pressure from 2.9 GPa to 3.5 GPa is shown in Figure 2a where LABs appear to be forming earlier. Figure 2b-e shows optical images of the different stages of LAB growth (LAB%) quantified in Figure 2a. For each tested bearing, two sections around the inner ring were analysed and the LAB% and HAB% were measured three times for each section. The average of the six measurements and their standard root-mean square deviation (error bar) have been shown in Figure 2a.

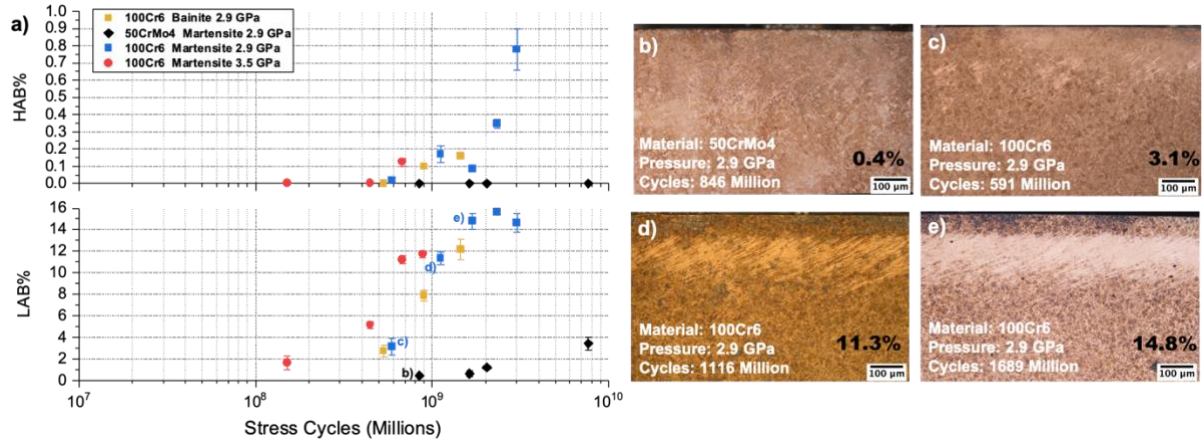

Figure 2: a) LAB% and HAB% recorded for each sample in this study under different stress cycles. Optical images of LABs from different stages in a) are shown in b),c),d) and e). Test conditions and LAB% value is shown for each optical image.

3.1 Saturation Level

According to the findings presented and discussed in **[3]**, the percentage of LABs formed in bearings varies with contact pressure and stress cycle but always forms within a band of depths in the bearing ring subsurface with an upper and lower boundary coincide with the 1300 MPa von Mises threshold, as illustrated in Figure 3. The upper and lower boundaries are assigned as y_1 and y_2 respectively, which vary with the contact pressure and can be determined by calculating the corresponding von Mises stress. The LAB% is found to reach a saturation level after sufficient number of cycles, this appears to be around 15 for the 100Cr6 under 2.9 GPa and is achieved after approximately 1700 million cycles (as shown in Figure 2). This percentage is thus referred to as the LAB saturation level, $LAB\%_{sat}$ (and will be employed later in Equation 9).

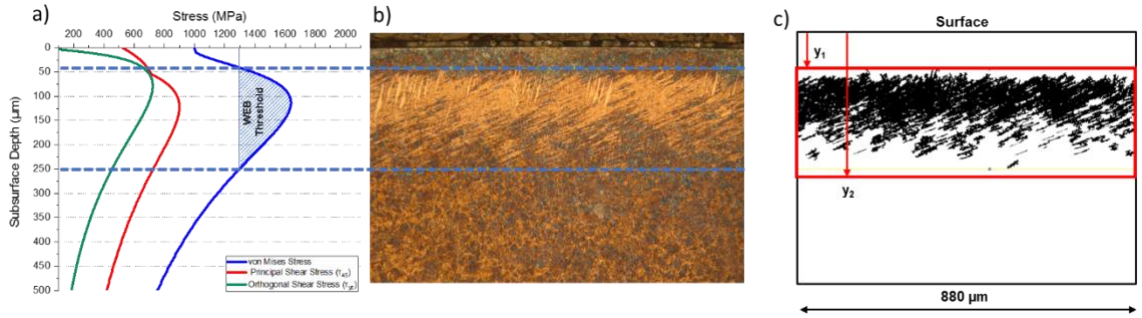

Figure 3: a) subsurface stress distribution for ACBB samples under 2.9 GPa. b) boundaries of WEBs in 100Cr6 martensite sample run for 3016 x10^6 cycles under 2.9 GPa which is considered at the saturation stage. c)the threshold zone highlighted in red in which the WEBs form within.

However, for the 100Cr6 material under 3.5 GPa, although the same LAB% growth trend is seen, an LAB saturation level was not reached, as shown in Figure 2, due to relatively low number of cycles [3]. Nonetheless, $LAB\%_{sat}$ could be calculated for the 3.5 GPa based on the threshold zone depth boundaries in which the WEBs form. Figure 3c shows the threshold zone (highlighted in red) which is determined based on the von Mises stress.

When comparing the area of LABs in the samples relative to the threshold zone (880 × (y_2 - y_1)), rather than the full optical image area, the maximum area of LABs achieved during the saturation level mentioned previously is found to be equivalent to 48% of this threshold zone (Equation 10). Under a different contact pressure, due to the change of von Mises stress the material is subject to, the maximum area of the LABs will change however its percentage in the threshold zone will be considered to remain same as that under 2.9 GPa (48%). Hence by using Equation 9 and 10, $LAB\%_{sat}$ is estimated to be 28 for the 3.5 GPa samples as the corresponding ($y_2 - y_1$) is 390 µm.

$$LAB\%_{sat} = \frac{Maximum\ LAB\ Area}{666.7 * 880} \times 100 \quad (9)$$

$$Maximum\ LAB\ Area = 0.48 \times (y_2 - y_1) \times 880 \quad (10)$$

By quantifying the LAB% under different stress cycles (experimentally) and determining the saturation level ($LAB\%_{sat}$) using Equation 9 and 10 under each contact pressure, the LAB evolution from its initiation to saturation can be modelled as detailed in the next section.

4. Modelling of WEB formations

Based on the experimental data points obtained for the 100Cr6 samples, a curve fitting is applied to derive the relationship between LAB density (LAB%) and stress cycles under 2.9 GPa and 3.5 GPa. Given the similarity between the bainitic and martensitic samples in Figure 2, this suggests that having RA varying from 2-5% does not have a significant influence on WEB formation. However, further investigation is required to quantify the influence of RA on WEB formation over a larger range. According to previous models [20, 13], where carbon atom mitigation and diffusion follows a sigmoidal pattern, and this was found to agree with the experimental data extremely well as shown in Figure 4, using the standard Boltzmann curve fitting equation as shown in Equation 11. The sigmoidal pattern derived from the experimental result is a typical relationship for diffusion processes.

$$LAB\% = \frac{A_1 - A_2}{1 + e^{\frac{(x - x_0)}{dx}}} + A_2 \quad (11)$$

Where x is the number of stress cycles, A_2 is the LAB saturation level ($LAB\%_{sat}$), x_0 is the number of cycles required to reach half of the LAB saturation level and A_1 is an offset value to start the curve at 0, i.e. no LABs at the beginning of a RCF testing. The value of dx is a time constant dependent on the linear slope m of the curve at $x = x_0$ as shown in Equation 12.

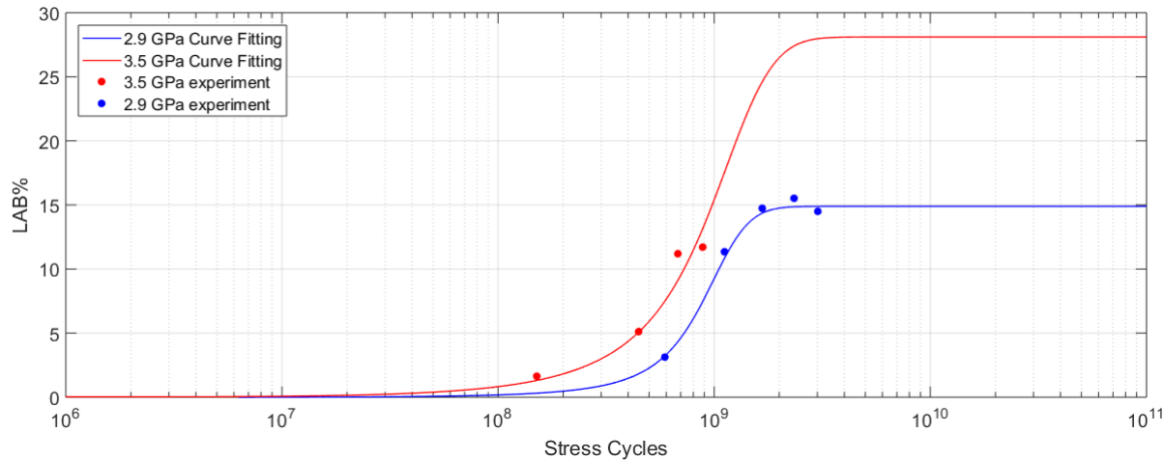

$$dx = \frac{A_2 - A_1}{4m} \tag{12}$$

Figure 4: LAB Density (LAB%) evolution curve fitting as a sigmoidal pattern with stress cycles for 2.9 GPa and 3.5 GPa for 100Cr6 martensitic bearing samples.

The curve fitting data for the 2.9 GPa and 3.5 GPa samples have been obtained using Origin 2018b and the constants for the 100Cr6 martensitic samples as well as those for intermediate contact pressures are given in Table 3, the intermediate values have been calculated through regression analysis. Firstly, the LAB saturation level A_2 is calculated using Equation (9) and Equation (10) for each pressure. Using the curves obtained for the samples under 2.9 GPa and 3.5 GPa and their corresponding constants, x_0 and dx are then determined directly through regression analysis as a function of contact pressure (see Appendix). Finally, the offset value A_1 is determined by applying the initial condition $LAB\% = 0$ when $x = 0$ to Equation 11.

Table 3: Calculated constants for the determination of the LAB Density curve fitting under contact pressures between 2.9 and 3.5 GPa based on logarithmic regression for 100Cr6 bearing steel samples.

Contact Pressure (GPa)	**x_0**	**dx**	**A_2**	**A_1**
2.9	8.71E+08	2.40E+08	15	-0.41
3	8.67E+08	2.61E+08	18	-0.65
3.1	8.63E+08	2.83E+08	20	-0.95
3.2	8.59E+08	3.08E+08	22	-1.35
3.3	8.55E+08	3.35E+08	24	-1.87
3.4	8.51E+08	3.64E+08	26	-2.50
3.5	8.47E+08	3.95E+08	28	-3.28

Although there are a number of regression methods available providing a variety of curve fittings for the pressures between the 2.9 and 3.5 GPa, based on a recent study that has demonstrated how the LAB initiation point varies with contact pressure [13], where a logarithmic curve fitting was applied, the same approach (detailed in Appendix A) is taken to determine the value of x_0 and dx for pressures other than 2.9 and 3.5 GPa. A plot of the obtained curve fittings for these pressures between 2.9 GPa and 3.5 GPa is shown in Figure 5. Similar to Fu et al., an arbitrary value of LAB% = 1% is selected as the LAB 'initiation' point (shown in Figure 5), where the density of the LABs becomes significant enough to become visible under LOM. Although this has shown to be much earlier than that predicted based on the experimental observations in this study (and will be discussed later), it provides a prediction compatible to other theoretical models [13].

Significant evidence has suggested that HAB forms from pre-existing LABs when their density reaches a certain level [3]. According to the experimental findings, the earliest HABs formed in the 100Cr6 bainite sample at 897 million cycles, which corresponds to a LAB level of 8 %, see Figure 2. No sample with a lower LAB% has shown to have developed HAB in this study, hence it is modelled to predict HAB initiation based on the curve fittings shown in Figure 5, where the number of cycles required to initiate HABs is when each curve reaches the 8% of LABs. According to the datapoints in Figure 2, the highest LAB% (=5%) without HAB is the 100Cr6 martensitic sample tested for 447 million cycles under 3.5 GPa. Therefore, it is likely that the actual HAB initiation point lies between 5-8% of LABs. Since 8% LAB is a confirmed result, it will be used to predict the initiation of HABs (shown in Figure 5). Given that the data range in this study were for the 2.9 GPa and 3.5 GPa contact pressures, the curves calculated have been limited to pressures within this range but may be extrapolated beyond this, which will be discussed in the next section.

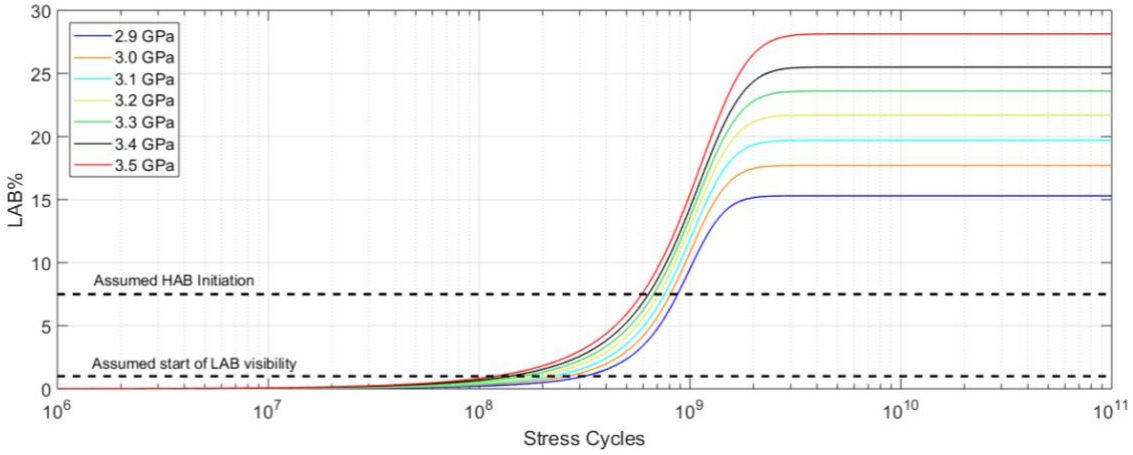

Figure 5: LAB% varies with stress cycles under contact pressures between 2.9 and 3.5 GPa (100Cr6) using the evolution modelling and showing initiation of LAB visibility in the subsurface when LAB% is 1% and HAB initiation when LAB% is 8%.

Based on the experimental data points for 50CrMo4M under 2.9 GPa shown in Figure 2, the same approach is adapted to model this material's LAB evolution, considering the LAB saturation level to be the same as 15%. As shown in Figure 6, a totally different prediction from that of the 100Cr6 is obtained, i.e. due to the much lower growth rate of LABs in this material, both the initiation and saturation of the LABs are predicted to occur after a much more numbers of stress cycles for this lower carbon steel. As discussed earlier, due to the similar behaviour (see in Figure 2a), that WEB evolution in the 100Cr6 bainite would have the same curve fitting as the martensite (see Figure 7a). Optical images of 100Cr6 martensite and bainite samples under similar stress cycles in Figure 7b-e show how comparable the growth rate of LABs are for both microstructure.

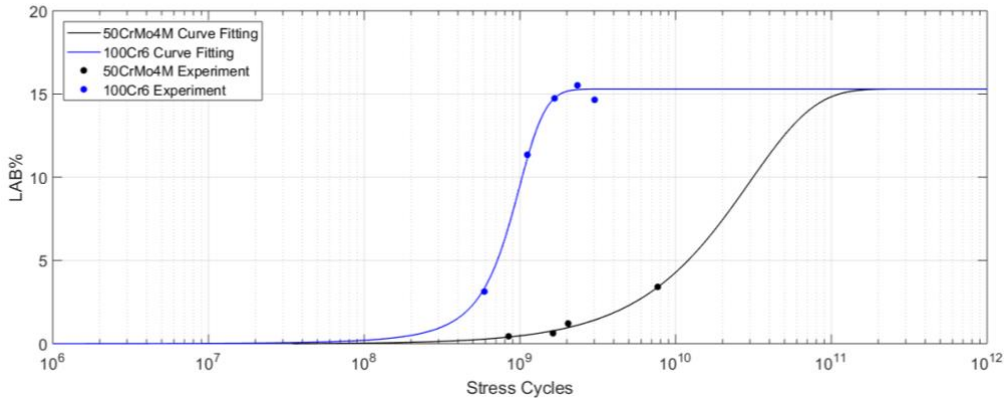

Figure 6: LAB Density evolution curve fitting as a sigmoidal pattern with stress cycles under 2.9 GPa for 100Cr6 and 50CrMo4M bearing samples

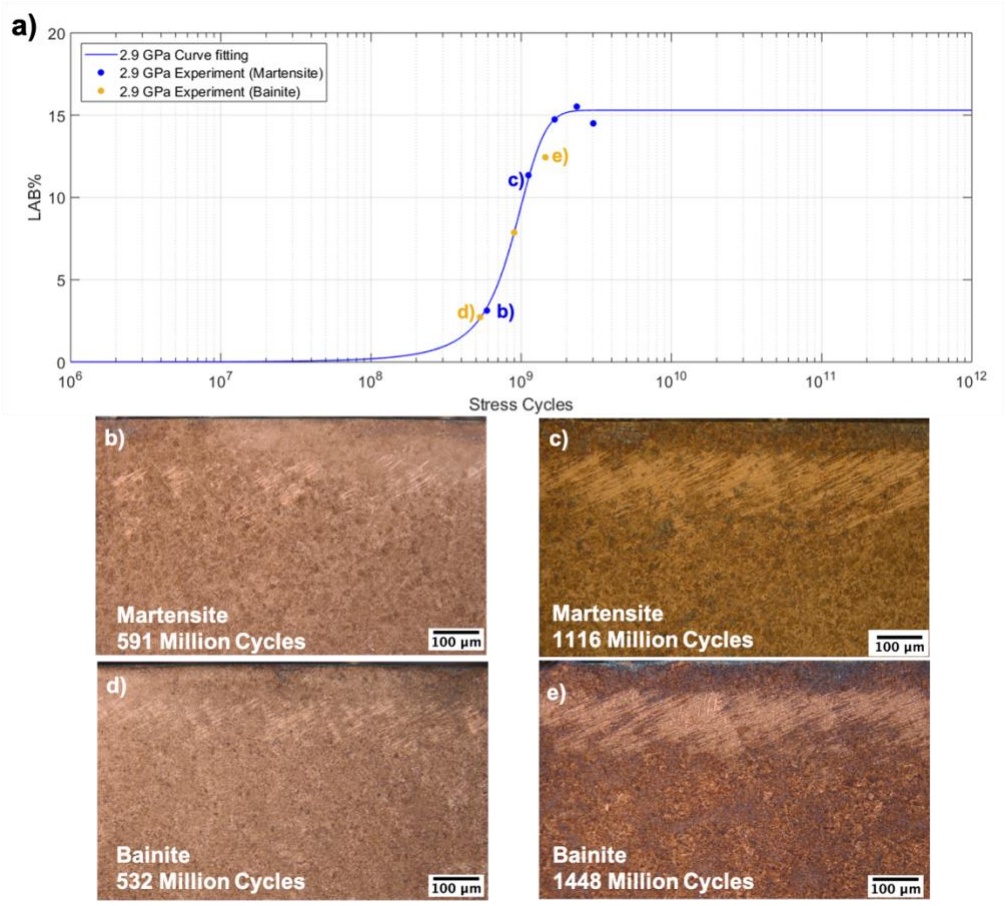

Figure 7: a) curve fitting and experimental data for 100Cr6 martensitic samples at 2.9 GPa compared to experimental data for 100Cr6 bainitic samples under 2.9 GPa. b,c,d,e)Optical images of LABs recorded from martensite and bainite 100Cr6 samples recorded in a).

The semi-empirical model is based on the following assumptions:

- The depth boundaries of saturated WEBs are defined by depths of the corresponding 1300 MPa von Mises stress threshold.
- At saturation, LAB% reaches 48% of the area defined by the 1300 MPa threshold.
- HAB formation begins when LAB% reaches 8%.

5. Discussion

WEBs have been reported to consist of ferrite grains (both cellular and elongated grains) and lenticular carbides that form adjacent to the bands [6]. However, the constituents of 'white' in WEBs have not been clearly defined in literature. LOM images have been compared to SEM images of LABs and HABs in an etched 100Cr6 martensitic sample tested under 3.5 GPa over 679 million cycles, a selected comparison is shown in Figure 8. It is observed that the white area is associated mainly with the cellular ferrite grains (red arrows) in the WEBs and the lenticular carbides (yellow arrow) appear to be dark in the LOM image. However, the appearance of white or dark colour of the LCs may be different when the direction of polarized light is adjusted in optical microscope. This has caused confusions as Nital etchant is expected to attack the relatively soft cellular ferrite and ferrite-

cementite grain boundaries **[6, 17]**, and it remains unclear why the reflectivity of cellular ferrites in WEBs give a white appearance whereas the ferrites in DERs give a dark appearance under same etching process **[2]**.

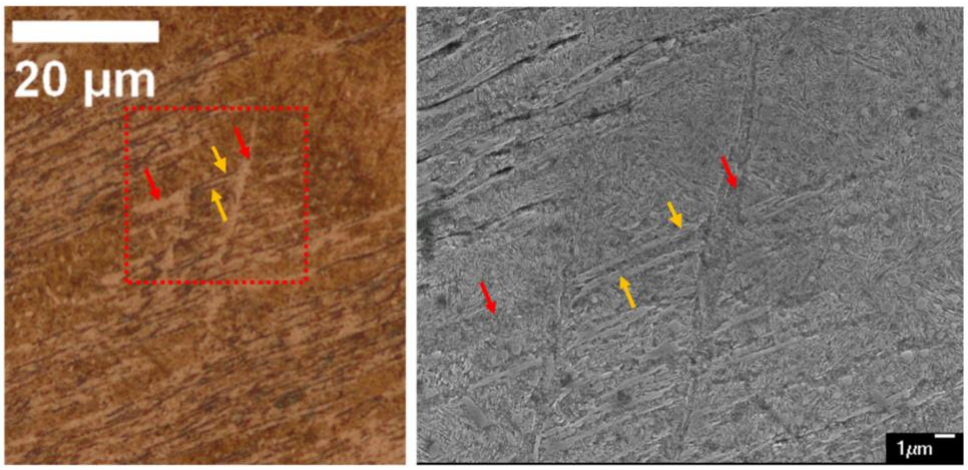

Figure 8: left) An optical image of an etched 100Cr6 martensite sample tested under 3.5 GPa over 679 x106 cycles, showing white bands (both LABs and HABs) formed in the sample. Right) The corresponding SEM image showing the area highlighted in red square of the optical image to show the LC (yellow arrow) and globular ferrite (red arrow) in both images.

Based on the findings from this work, the modelling has been based on the white area in LABs and HABs that is attributed to the ferrite grains formed in the steel microstructure as opposed to other models [13, 14, 20, 1] based on the thickening of LCs adjacent to individual LABs due to carbon diffusion.

The most recent model for microstructural alterations by Fu et al. [13] is based on the thickening of nano-sized tempered carbides for DER and on thickening of LC for LABs. The evolution of the LC thickness over stress cycles follows a sigmoidal pattern similar to that of the LAB ferrite area in this study. Different from the modelling of carbide thickening of individual band in most literature, a semi-empirical model based on the overall white etched areas growth in WEBs is proposed from this study. Nonetheless, the growth of white etched areas in the LABs may be proportional to the dislocation-assisted carbon migration causing the carbide thickening, leading to the similar prediction patterns from both approaches.

Figure 9 presents a comparison of the curve fitting predicted by the semi-empirical model from this study with that established from the LC thickening model proposed by Fu et al. [13] under 2.9 GPa. The semi-empirical model in this study shows that LABs form much earlier than that predicted by Fu's model. This is expected since the semi-empirical model prediction is based on the measurement of the white etched areas of WEBs, i.e. cellular ferrite formation while Fu's model focuses on the formation of lenticular carbides (LC). It is believed that the cellular ferrite (white area) forms prior to the LC. The carbon migration in the material (either due to dislocation gliding or diffusion of free carbon) contributes to the nucleation and thickening of LCs. This carbon migration occurs due to the inability of the ferrite grains (associated with the LABs) to dissolve the excess carbon from the

parent microstructure (carbon solubility in ferrite is 0.02%wt). Therefore, it is assumed that prior to LC formation, there exists an LAB that is purely ferrite supersaturated with carbon. This excess carbon later migrates away to form LCs. This is supported by the comparison between the LC thickening model [13] and the semi-empirical model of this study with the latter predicting earlier LAB formation than the former. The sigmoidal pattern established in this study and by Fu et al. [13] suggests the WEB formation mechanism is driven by a diffusion process. However, the variation in the curve distribution between the two studies leads to uncertainties in the proposed driver for WEB formation in literature.

Given the nature of a sigmoidal curve, i.e. no definitive point for approaching 0% LAB, Fu et al. [13] took an arbitrary value of 1% of the number of cycles for the curve to fully saturate as the LAB initiation point, i.e. at $1.2x10^9$ stress cycles (as shown in Fig.9). This is much later than the semi-empirical model has predicted at $3.15x10^8$, which has been demonstrated by experimental observations. Two samples, after $5.91\ x10^8$ and $1.116\ x10^9$ stress cycles, have shown to have formed LABs as shown in Figure 2.

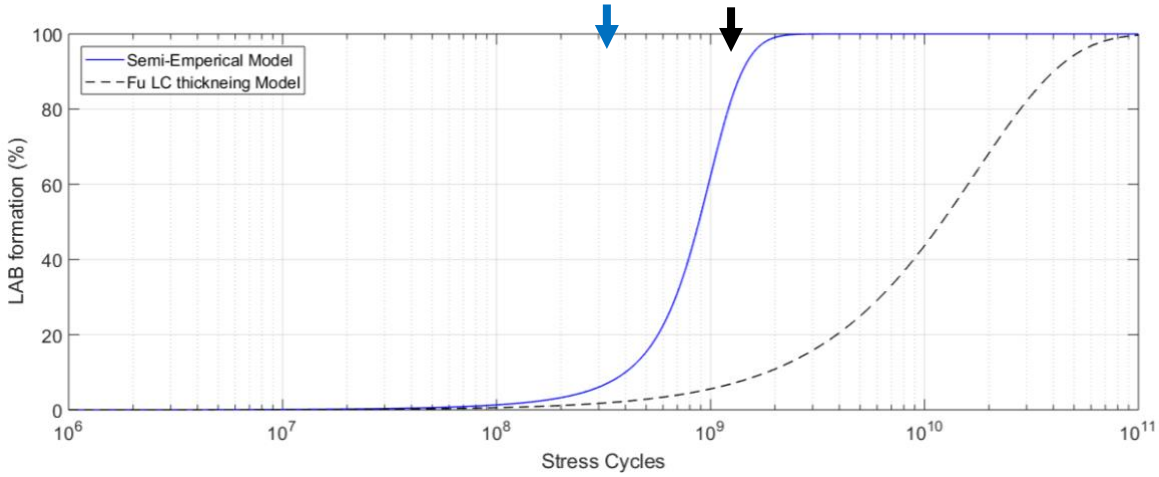

Figure 9: A comparison of the LAB prediction models between the semi-empirical model from this study and the model by Fu et al based on LC thickening [11] under 2.9 GPa (normalized to 0-100% LAB). Blue and black arrow shows the LAB initiation point based on the semi-empirical modal in this study and the LC thickening model respectively.

A similar comparison is made for the higher contact pressure under 3.5 GPa (see in Figure 10). Although the two curves are closer, the model by Fu et al. still predicts LAB initiation much later than the semi-empirical model from this study, i.e. $1.2\ x10^8$ cycles vs. $2.6\ x10^8$, due to similar reasons as discussed above. However under high contact pressure, the migration of carbon driven by dislocations would be faster thus the two curves become closer.

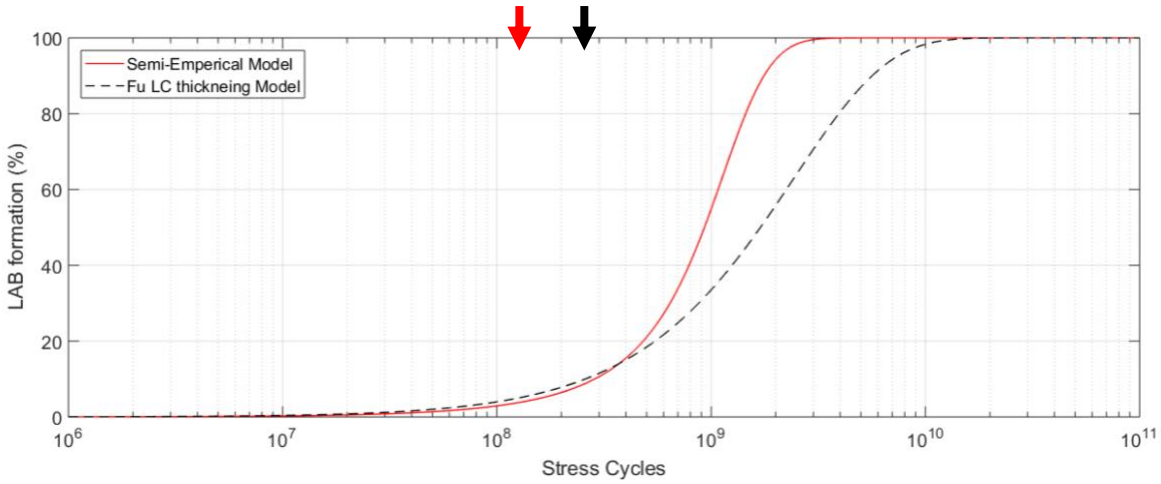

Figure 10: A comparison of the LAB prediction models between the semi-empirical model from this study and the model by Fu et al based on LC thickening [13] under 3.5 GPa (normalized to 0-100% LAB) . Red and black arrow shows the LAB initiation point based on the semi-empirical modal in this study and the LC thickening model respectively.

A comparison of the LAB initiation predictions under a range of contact pressures made by the semi-empirical model and Fu's model is shown in Figure 11. Fu's hypothesis arbitrarily assumes the initiation point as 1% of the stress cycles required to reach LAB saturation. The semi-empirical model differs as it predicts the point when the LAB% is 1% (i.e. certain LAB area is achieved) is the LAB initiation and this is calculated from the sigmoidal fitting, this has been taken as this is practically where LAB(s) can be distinguished from the surrounding microstructure under LOM. Although still not definitive, it has been demonstrated by experimental observations. The actual initiation point might be even earlier considering the initiation of LAB is caused by nano to micro-size cellular ferrite grain formation. The sigmoidal relationship obtained from the experimental data in this study supports a diffusion mechanism leading to WEB formation. Under this process, there is no definitive point as to when the features initiate therefore it is only when the features become sufficiently developed that it can be seen (assumed when LAB% is 1% in this study).

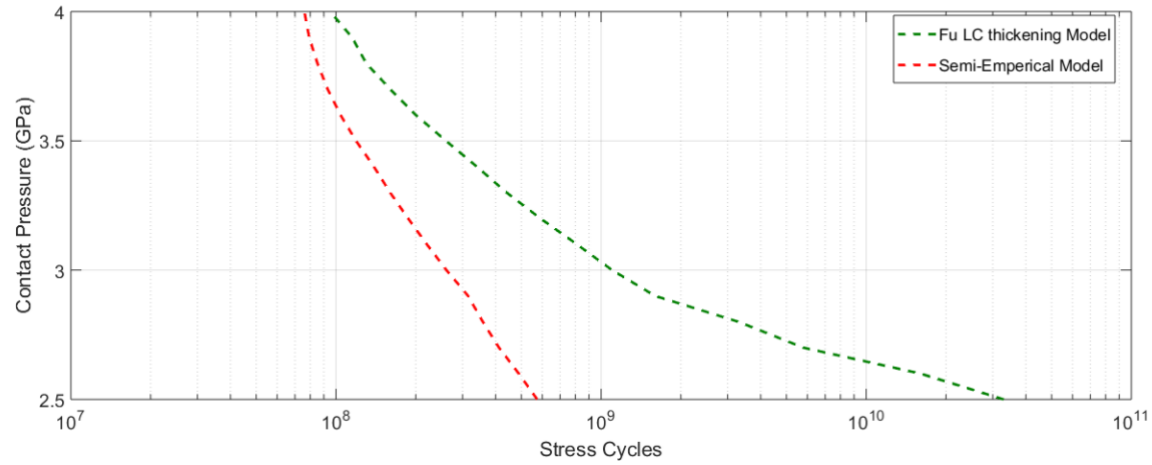

Figure 11: A comparison of the LAB initiation predictions made by the semi-empirical model and Fu's model [11] under a range of contact pressures.

It is commonly proposed in literature that a contact pressure of 2.5 GPa (approximate shakedown limit for 100Cr6) is the threshold pressure for the formation of microstructural alterations such as WEBs **[2]**. This would suggest the initiation curve shown in Figure 11 would approach asymptotically at 2.5 GPa. This was not observed in the semi-empirical curve for the LAB initiation in this study due to the regression analysis limitation of the data range between 2.9 GPa - 3.5 GPa being extrapolated to 2.5 GPa – 4 GPa. However, there is limited experimental studies in literature examining WEBs at low contact pressure to further investigate this and compare.

Although no prediction models have been found in literature, it is generally agreed that HABs form from pre-existing LABs [3, 22, 23, 24, 8, 5, 11, 25, 15, 26] [9]. The experimental results in this study have shown that HABs form when LAB% reaches to 8%, which has thus been used to predict HAB formation. Given the LAB% for the 50CrMo4M in this study remained under 5%, this would explain why no HABs were observed in 50CrMo4M samples in this study. Figure 12 shows the LAB and HAB prediction curves for 100Cr6 based on the semi-empirical models developed compared to both experimental data points from this study and those from literature, demonstrating that the models have accurately predicted both LABs and HABs formation in 100Cr6 bearing steels in the majority of cases. One 'no WEB' case from literature falls into the LAB region and three LAB cases from literature fall into the HAB region. However, all of the other 27 data points have been correctly predicted by the LAB and HAB semi-empirical models despite the uncertainties on their operating conditions and material heat treatment. Since the models are based on constant operating temperature and bearing rotating speed, their influence on LABs and HABs are not considered in these models. Further work is being conducted to add these variables in the models in the near future.

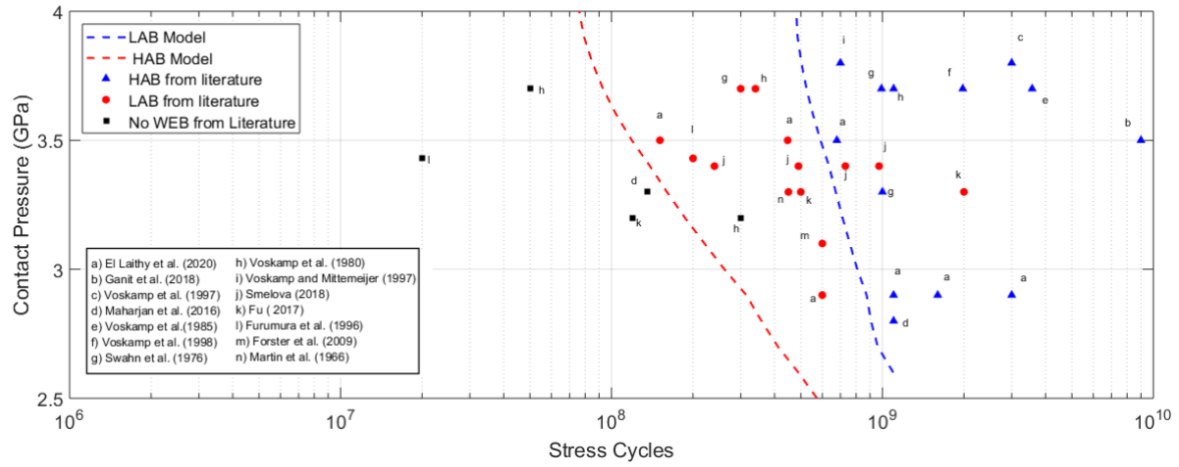

Figure 12: Predictions of LAB and HAB initiation based on the semi-empirical models developed in this study incorporating experimental LAB and HAB formation results from literature. Note: points marked as 'no WEB' indicates RCF tests did not result WEBs but some have had DER formed.

As discussed earlier, the Bainitic 100Cr6 (containing 2% retained austenite) performs similarly to its Martensitic version (containing 5% retained austenite) hence same models can be applied. This also suggests that the change of retained austenite in the 100Cr6 bearing steel (2-5%) does not have significant influence on WEB formation. However, it is possible that large RA contents (>5%) may yet influence WEB formation. It is interesting that the low carbon steel (50CrMo4M) showed a much delayed WEB formation and growth comparing with the 100Cr6 steel, hence a different prediction model is applied for each material. It suggests that lowering the carbon content in the steel may significantly delay the formation of LABs due to reduction of the driving force in the material for carbon diffusion and LC thickening which consequently impedes HAB formation.

Furthermore, a comparison between literature experimental data and the semi-empirical predictive model under a certain contact pressure (3.3 GPa) is made, where the WEB formation progress model is compared in terms of the upper and lower boundaries of the WEB region. Using the y_1 and y_2 boundaries (defined by the relevant von Mises stress as described above) as the maximum width of the WEBs ($y_2 - y_1$) and comparing this to the WEB boundaries reported in literature at different cycles, The data points shown in Figure 13 indicate the reported WEB width as a percentage of the maximum width ($y_2 - y_1$). One of the data point in the graph shows 0% from Maharjan et al. [5] as no WEB was found to have formed under the designated conditions. It can be seen that the model has closely predicted the WEB formations under this contact pressure. The deviation observed may be attribute to the small variations from the experimental conditions, e.g. Martin et al. [9] and Swahn et al. [11] used a relatively lower operating temperature of 50°C while the model is based on the 80°C tests in this study. Also Fu et al. [15] tested a material with a significantly higher heat treatment (time and temperature) hence the material was softer than that in this study which may have an impact on the formation of the features.

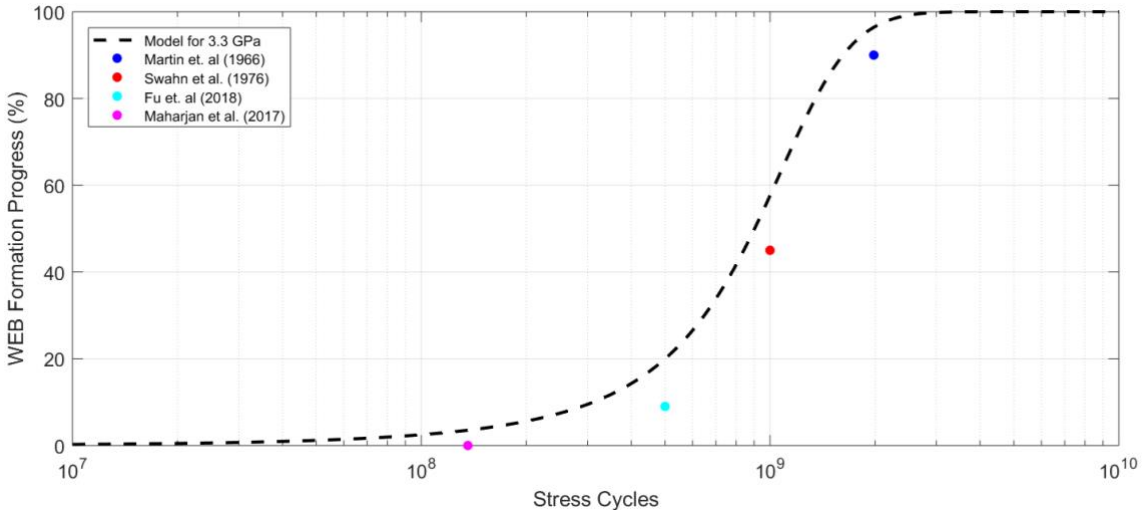

Figure 13: A comparison of WEB formation progress as a percentage of the formed WEB in the expected saturated WEB with the normalized LAB% evolution curve from the semi-empirical model under 3.3 GPa.

6. Conclusions

A large amount of experimental data obtained from the investigation of WEB formation mechanisms in bearing steels provides a unique opportunity for developing a predictive model for WEBs in this study. Based on the density of LABs and HABs formed in the bearing steels under different contact pressures over a range of stress cycles, semi-empirical models have been proposed to predict the initiation and evolution of LABs and HABs for martensitic and bainitic 100Cr6, as well as a low carbon steel 50CrMo4M, under contact pressures ranging from 2.9 GPa to 3.5 GPa. This is achieved by quantifying the area covered by the WEB network at different stages over hundreds on microns of the material subsurface which provides a more practical overview of the material response during RCF on a global scale compared to previous models comparing the thickness of individual bands at a local scale. This study has successfully modelled the WEB features and establishing a link between LABs and HABs. Although a link between LABs and HABs formation have been proposed in literature **[3]** , no model has successfully established a link between LABs and HABs. The models have shown to agree extremely well with other experimental data from literature. Key conclusions from this study are:

- The latest LAB prediction models proposed in literature do not agree with the experimental findings from this study, e.g. the LABs in this study appear to form much earlier than the predicted WEB formation models based on LC thickening.
- Data points in this study show the growth of LABs to follow a sigmoidal pattern fitted using a Boltzmann curve fitting. The growth pattern supports the theory that WEB formation is driven by a diffusion process. However, the driver of the process may be different to the dislocation gliding model proposed in literature due to the difference in growth pattern compared to this study.
- A unified WEB% based on von Mises stress threshold at 1300 MPa is introduced to quantify the evolution of LABs and HABs as opposed to the LC thickness used in other models.
- A semi-empirical model based on the LAB% vs. stress cycles under 2.9 GPa and 3.5 GPa has been established to predict LABs evolution under other pressures within this range. The model has shown to agree very well with experimental data from literature.
- Based on the assumption of 1% LABs is observable under LOM, initiation of LABs (when they can be seen under LOM) is predicted and a LAB initiation prediction model has been established.
- Based on experimental findings that 8% LAB (area of LABs relative to a fixed reference area) would

promote initiation of HABs, a semi-empirical model is established to predict the initiation of HABs over the contact pressure range of 2.9 and 3.5 GPa.

- The evolution of WEBs vs stress cycles has been shown to be very similar for martensitic and bainitic 100Cr6 while the low carbon 50CrMo4M shows a significant delay in WEB formation.

7. Acknowledgement

This research has been co-funded by ESPRC (EP/N509747/1) and Schaeffler Technologies AG & Co. KG, Schweinfurt, Germany.

8. Appendix

Trendline equation y = A + Bln(x) where y is the contact pressure in GPa, x is variable being analysed (x_0 or dx) and A,B are constants to be determined.

$$\boldsymbol{B = \frac{S_{xy}}{S_{xx}}} \quad , \qquad \boldsymbol{A = \bar{y} - B\overline{ln(x)}}$$

$$\boldsymbol{S_{xx} = \sum [ln(x_i)]^2 - n * \overline{ln(x)}^2} \quad , \qquad \boldsymbol{S_{xy} = \sum ln(x_i y_i) - n * \overline{ln(x)} * \bar{y}}$$

References

[1] I. A. Polonsky and L. M. Keer, “On white etching band formation in rolling bearings,” Journal of the Mechanics and Physics of Solids, vol. 43, pp. 637-669, 1995.

[2] M. El Laithy, L. Wang, T. J. Harvey, B. Vierneusel, M. Correns and T. Blass, “Further understanding of rolling contact fatigue in rolling element bearings-a review,” Tribology International, vol. 140, p. 105849, 2019.

[3] M. El Laithy, L. Wang, T. Harvey and B. Vierneusel, “ Re-investigation of dark etching regions and white etching bands in SAE5 2100 bearing steel due to rolling contact fatigue,” International Journal of Fatigue, vol. 136, p. 105591, 2020.

[4] H. Fu and P. E. J. Rivera-Díaz-del-Castillo, “Evolution of White Etching Bands in 100Cr6 Bearing Steel

under Rolling Contact-Fatigue," Metals, vol. 9, p. 491, 2019.

[5] N. Maharjan, W. Zhou and Y. Zhou, "Micro-structural study of bearing material failure due to rolling contact fatigue in wind turbine gearbox," in Proceedings of the international symposium on current research in hydraulic turbines, Kathmandu University, Dhulikhel, Nepal, 2016.

[6] V. Šmeļova, A. Schwedt, L. Wang, W. Holweger and J. Mayer, "Electron microscopy investigations of microstructural alterations due to classical Rolling Contact Fatigue (RCF) in martensitic AISI 52100 bearing steel," International Journal of Fatigue, vol. 98, pp. 142-154, 2017.

[7] H. Fu, W. Song, E. I. Galindo-Nava and P. E. J. Rivera-Díaz-del-Castillo, "Strain-induced martensite decay in bearing steels under rolling contact fatigue: modelling and atomic-scale characterisation," Acta Materialia, vol. 139, pp. 163-173, 2017.

[8] A.Voskamp, "Material Response to rolling contact loading," Journal of Tribology, vol. 107, pp. 359-364, 1985.

[9] J. A. Martin, S. F. Borgese and A. D. Eberhardt, "Microstructural alterations of rolling—bearing steel undergoing cyclic stressing," Journal of Basic Engineering, vol. 88, pp. 555-565, 1966.

[10] J. J. Bush, W. L. Grube and G. H. Robinson, "Microstructural and Residual Stress Changes in Hardened Steel due to Rolling Contact," Transactions of the ASM, vol. 54, pp. 390-412, 1961.

[11] H. P. C. O. Swahn, P. C. Becker and O. Vingsbo, "Martensite decay during rolling contact fatigue in ball bearings," Metallurgical transactions A, vol. 7, pp. 1099-1110, 1976.

[12] A. P. Voskamp, "Microstructural stability and bearing performance," in Bearing Steel Technology, ASTM International, 2002.

[13] H. Fu and P. E. J. Rivera-Díaz-del-Castillo, "A unified theory for microstructural alterations in bearing steels under rolling contact fatigue," Acta Materialia, vol. 155, pp. 43-55, 2018.

[14] J. Buchwald and R. W. Heckel, "An analysis of microstructural changes in 52100 steel bearings during cyclic stressing(Microstructural changes in 52100 steel bearing inner rings during cyclic stressing, obtaining thickening rate data on white-etching regions and lenticular carbides)," ASM Transactions

Quarterly, vol. 61, pp. 750-756, 1968.

[15] H. Fu, Microstructural alterations in bearing steels under rolling contact fatigue, University of Cambridge, Doctoral Thesis, 2017.

[16] A. Warhadpande, F. Sadeghi and R. D. Evans, “Microstructural Alterations in Bearing Steels under Rolling Contact Fatigue: Part 2—Diffusion-Based Modeling Approach,” Tribology Transactions, vol. 57, pp. 66-76, 2013.

[17] A. Warhadpande, F. Sadeghi and R. D. Evans, “Microstructural alterations in bearing steels under rolling contact fatigue Part 1—Historical overview,” Tribology Transactions, vol. 56, pp. 349-358, 2013.

[18] E.Orowan, “Mechanical strength properties and real structure of crystals,” Kristallogr, vol. 89, pp. 327-343, 1934.

[19] A.Cotrell and B.Bilby, “Dislocation theory of yielding and strain ageing of iron,” Proceedings of the Physical Society, Section A, vol. 62, no. 1, p. 49, 1949.

[20] J. Kang, Mechanisms of microstructural damage during rolling contact fatigue of bearing steels, University of Cambridge , Doctoral Thesis, 2014.

[21] D. Markus and T. Werner, “Influence of Sulfur Inclusion Content on Rolling Contact Fatigue Life,” Bearing Steel Technologies: Advances in Steel Technologies for Rolling bearings, vol. 10, pp. 83-99, 2014.

[22] S. Ganti, B. Turner, M. Kirsch, D. Anthony, B. McCoy, H. Trivedi and V. Sundar, “Three-dimensional (3D) analysis of white etching bands (WEBs) in AISI M50 bearing steel using automated serial sectioning,” Materials Characterization, vol. 138, pp. 11-18, 2018.

[23] A. P. Voskamp, R. Österlund, P. C. Becker and O. Vingsbo, “Gradual changes in residual stress and microstructure during contact fatigue in ball bearings,” Metals Technology, vol. 7, pp. 14-21, 1980.

[24] N. H. Forster, L. Rosado, W. P. Ogden and H. K. Trivedi, “Rolling contact fatigue life and spall propagation characteristics of AISI M50, M50 NiL, and AISI 52100, Part III: metallurgical examination,” Tribology Transactions, vol. 53, pp. 52-59, 2009.

[25] V. Rumpf, A study on Microstructural Alterations in White Etching Cracks, Dark Etching Region, and White Etching Bands in Rolling Contacts, University of Southampton, Doctoral Thesis, 2018.

[26] K. Furumura, M. Yasuo and A. Tsutomu, “Development of long life bearing steel for full film lubrication and for poor and contaminated lubrication,” Motion Control 1, pp. 30-36, 1996.